

# Structure and diffusion of molten alkali carbonate salts at the liquid-vacuum interface

Gerrick E Lindberg <sup>Corresp. 1, 2, 3</sup>

<sup>1</sup> Department of Chemistry and Biochemistry, Northern Arizona University, Flagstaff, AZ, United States

<sup>2</sup> Department of Applied Physics and Material Science, Northern Arizona University, Flagstaff, AZ, United States

<sup>3</sup> Center for Materials Interfaces in Research and Applications, iMIRA!, Northern Arizona University, Flagstaff, AZ, United States

Corresponding Author: Gerrick E Lindberg

Email address: gerrick.lindberg@nau.edu

The liquid-vacuum interface of molten alkali carbonate salts is studied with molecular dynamics simulations. Three salts comprised of  $\text{Li}_x\text{Na}_y\text{K}_z\text{CO}_3$  near their respective eutectic concentrations are considered to understand the distribution of ions relative to a liquid-vacuum interface and their diffusivity. These simulations show that each of the cations accumulate at the interface preferentially compared to carbonate. The cation ordering is found to inversely correspond to cation radius, with K being the most likely occupant at the surface, followed by Na, Li, and then the anion. Similar to other studies, the carbonate is found to diffuse more slowly than the cations, but we do observe small differences in diffusion between compositions that present opportunities to optimize ion transport. These results hold consequences for our understanding of ion behavior in molten carbonate salts and the performance of devices employ these electrolytes.

1 **Structure and diffusion of molten alkali carbonate salts at the liquid-vacuum interface**

2 Gerrick E. Lindberg

3 Department of Applied Physics and Material Science

4 Department of Chemistry and Biochemistry

5 Center for Materials Interfaces in Research and Applications, iMIRA!

6 Northern Arizona University, Flagstaff, AZ, USA

7

8 Corresponding Author: Gerrick E. Lindberg

9 Email address: [gerrick.lindberg@nau.edu](mailto:gerrick.lindberg@nau.edu)

10

## Structure and diffusion of molten alkali carbonate salts at the liquid-vacuum interface

Gerrick E. Lindberg

Department of Applied Physics and Material Science

Department of Chemistry and Biochemistry

Center for Materials Interfaces in Research and Applications, iMIRA!

Northern Arizona University, Flagstaff, AZ, USA

[gerrick.lindberg@nau.edu](mailto:gerrick.lindberg@nau.edu)

### ABSTRACT

The liquid-vacuum interface of molten alkali carbonate salts is studied with molecular dynamics simulations. Three salts comprised of  $\text{Li}_x\text{Na}_y\text{K}_z\text{CO}_3$  near their respective eutectic concentrations are considered to understand the distribution of ions relative to a liquid-vacuum interface and their diffusivity. These simulations show that each of the cations accumulate at the interface preferentially compared to carbonate. The cation ordering is found to inversely correspond to cation radius, with K being the most likely occupant at the surface, followed by Na, Li, and then the anion. Similar to other studies, the carbonate is found to diffuse more slowly than the cations, but we do observe small differences in diffusion between compositions that present opportunities to optimize ion transport. These results hold consequences for our understanding of ion behavior in molten carbonate salts and the performance of devices employ these electrolytes.

**Keywords:** molten alkali carbonate salts, liquid-vacuum interface, molecular dynamics

### INTRODUCTION

Molten carbonate salts have been studied in many contexts because of their occurrence in natural environments, in many engineered materials, and as components in various devices (Gaune-Escard & Haarberg, 2014). Alkali carbonate melts specifically are attractive for use in many applications because they have low vapor pressures, are easy to contain, and are generally environmentally safe (Maru, 1984; Gaune-Escard & Haarberg, 2014). A significant amount of interest has been motivated by electrochemical devices and chemical separation technologies, which can be designed to have high efficiency, resilience from fouling, and low material costs (Maru, 1984; Dicks, 2004; Kirubakaran, Jain & Nema, 2009; Wade et al., 2011; Roest et al.,

42 2017). The performance of such devices have been studied in addition to the bulk behavior of  
43 individual components of relevant systems, but the thermodynamics and dynamics of alkali  
44 carbonate electrolytes near the relevant interfaces are not as well understood. The behavior of  
45 interfaces generally, and ions at liquid-vacuum interfaces, have received significant attention as  
46 regions featuring interesting manifestations of physical principles and as domains where distinct  
47 chemistries can occur (Allara, 2005; Kumar, Knight & Voth, 2013; Soniat, Kumar & Rick, 2015;  
48 Tse et al., 2015; Bastos-González et al., 2016; Gutiérrez et al., 2018). The purpose of this work is  
49 to apply similar methods to characterize the liquid-vacuum interface of three molten alkali  
50 carbonate electrolytes.

51         These electrolytes present many aspects that are of a general interest to chemists in many  
52 subdisciplines. Their performance and feasibility for use in molten carbonate fuel cells is of  
53 particular relevance because the operation of such devices relies on both the structure and  
54 transport of molecules at interfaces and the bulk within the device. In a typical molten carbonate  
55 fuel cell oxygen and carbon dioxide gases are fed to the cathode where  $O_2$  is reduced and  
56 carbonate is formed. The carbonate ion is then transported through the electrolyte to the anode  
57 where carbonate reacts with hydrogen gas. The hydrogen is reduced, carbon dioxide is reformed,  
58 and water is produced. Therefore, the performance of these fuel cells depend on the efficient  
59 uptake of feed gases at an interface, transport of carbonate through the bulk electrolyte, and  
60 release of product gases at an interface. It is therefore important to characterize the bulk and  
61 interfacial behavior of these electrolytes.

62         Numerous computational studies have considered the bulk behavior of ion transport in  
63 these electrolytes (Habasaki, 1990; Koishi et al., 2000; Costa, 2008; Vuilleumier et al., 2014;  
64 Ottochian et al., 2016; Corradini, Coudert & Vuilleumier, 2016). Habasaki studied carbonate  
65 salts with Li or Na cations and found that the anion is significantly more mobile with the smaller  
66 cation, which they found is related to the ionic radii (Habasaki, 1990). Koishi and coworkers  
67 looked at carbonate salts with Li and K cations and found that carbonate diffusion is maximized  
68 when Li proportion is highest (Koishi et al., 2000). Costa and Ribeiro also found that carbonate  
69 diffuses fastest when there is more Li than K, but their trend is less clear, which they attribute to  
70 a small box size and higher system density (Costa, 2008). Corradini and coworkers generally  
71 found behavior of Li and K carbonate salts similar to other works, but interestingly postulated  
72 that ionic diffusion of cations and anions might be anticorrelated resulting in smaller ionic

73 conductivities than would be anticipated from the diffusion constants and the Nernst-Einstein  
74 relationship (Tissen, Janssen & Eerden, 1994; Corradini, Coudert & Vuilleumier, 2016), which  
75 was also observed by Vuilleumier et al. (Vuilleumier et al., 2014). These studies, however, do  
76 not consider the thermodynamics or transport of alkali carbonate salts in the interfacial regions  
77 that are important for the transport of ions through electrochemical devices.

78 Interfacial behavior of these molten alkali carbonate salts has been considered in a few  
79 studies (Roest et al., 2017; Gutiérrez et al., 2018, 2019). Roest and coworkers studied the  
80 behavior of Li, Na, and K carbonate salts at charged and neutral interfaces (Roest et al., 2017).  
81 They identify distinct mass and charge profiles in the molten liquid near the interface and the  
82 ions are found to diffuse more slowly in close vicinity of the interface. Gutiérrez et al. have  
83 studied molten  $\text{LiCO}_3$  and a eutectic mixture of  $\text{LiNaKCO}_3$  at an interface with carbon solids,  
84 gases, and vacuum (Gutiérrez et al., 2018, 2019). They find that the ions do arrange at the  
85 interface as defined by the Gibbs dividing surface. The Li and carbonate ions are found to have  
86 similar profiles outside of the Gibbs dividing surface (in the vacuum region), but Li and  
87 carbonate are found to be weakly layered below the interface in the liquid. In molten  $\text{LiNaKCO}_3$ ,  
88 they find a more complicated distribution of ions. The K is found to be most prevalent in the  
89 region outside the Gibbs dividing surface, and Li and Na are found just inside the Gibbs dividing  
90 surface. These studies leave questions about how salt composition affect ion and interface  
91 structure and dynamics.

92 It is with this in mind that this study examines the behavior of carbonate ions at a liquid-  
93 vacuum interface. In this work, the structure and transport of molten Li, Na, and K containing  
94 carbonate salts are examined at the liquid-vacuum interface. We carefully examine local density  
95 profiles with respect to the interface using two definitions of the divide between the liquid and  
96 vacuum. We also estimate the slab width, surface tension, and self-diffusion constant, and relate  
97 the observed values to the system composition.

98

## 99 METHODS

100 Simulations were performed of three eutectic systems with chemical formulas of the form  
101  $\text{Li}_x\text{Na}_y\text{K}_z\text{CO}_3$ , where  $x + y + z = 2$ . Redox processes are not considered in this work, so Li, Na,  
102 and K always refer to the cations and C and O to the constituents of the carbonate anion, which  
103 comprise the electrolyte. The fractions of each cation in each system considered in this work are

104 listed in Table 1. Cation fractions instead of mole fraction or concentration are used to emphasize  
105 the relative cation amounts in each system. The three systems considered have unique elemental  
106 compositions ( $\text{LiNaCO}_3$ ,  $\text{LiKCO}_3$ , or  $\text{LiNaKCO}_3$ ), so the alkali metal subscripts are dropped to  
107 simplify identification. These systems have been selected because they are near the eutectic  
108 compositions (Janz, 1967), which permits for the salt to be molten and for device operation at the  
109 lowest temperatures.

110 Initial configurations were prepared by placing 1000 cations (according to the fractions in  
111 Table 1) and 500 carbonate anions randomly on a grid in a simulation cell with dimensions of 40  
112 Å x 40 Å x 100 Å. The ions are positioned near the liquid density so they form a so-called *slab*  
113 of liquid surrounded by a large vacuum region. The system is constructed so that the average  
114 liquid-vacuum interface is perpendicular to the z-axis. This study uses the interaction parameters  
115 developed by Tissen and Janssen (Tissen & Janssen, 1990; Janssen & Tissen, 1990), sometimes  
116 called the JT model, which have been employed for many similar studies of molten alkali  
117 carbonate salts and as such provide a robust body of literature for validation and reference  
118 (Tissen & Janssen, 1990; Janssen & Tissen, 1990; Tissen, Janssen & Eerden, 1994; Koishi et al.,  
119 2000; Ottochian et al., 2016; Wilding et al., 2016; Roest et al., 2017; Du et al., 2017, 2019; Ding  
120 et al., 2018; Gutiérrez et al., 2018). Simulations were performed with the LAMMPS molecular  
121 dynamics package (Plimpton, 1995). The temperature was held constant using the Nosé-Hoover  
122 algorithm with a damping parameter of 500 fs and carbonate was kept rigid using the SHAKE  
123 algorithm as implemented in LAMMPS. Each system was heated from 0 to 1200 K in 50 ps and  
124 then equilibrated at 1200 K for 50 ps with a time step of 0.05 fs in the constant number of  
125 particles, temperature, and volume (NVT) ensemble. They were then further equilibrated in the  
126 NVT ensemble for 20 ns with a timestep of 0.5 fs. Finally, the thermodynamic data presented  
127 was extracted from 10 ns NVT production simulations and the diffusion constants from 10 ns  
128 constant number of particles, volume, and energy (NVE) simulations.

129 Molecular visualization was performed with VMD (Humphrey, Dalke & Schulten, 1996).  
130 Density profiles were calculated with in house scripts. Densities are normalized by dividing by  
131 the average density in the center of the respective slab to facilitate comparison between systems  
132 with different compositions. The Gibbs dividing surfaces are determined from the z-dimension  
133 density profile to find the two planes (one on each side of the slab) where the density is half the  
134 average bulk liquid density (Gochenour, Heyert & Lindberg, 2018). The instantaneous interfaces

135 were calculated with an in-house script using the method described in the work by Willard and  
136 Chandler (Willard & Chandler, 2010) using a coarse graining length,  $\xi$ , of 1.5 Å. Self-diffusion  
137 constants are determined from the mean-squared displacement as calculated by CPPTRAJ with  
138 the Einstein relation (Roe & Cheatham, 2013).

139

## 140 **RESULTS AND DISCUSSION**

### 141 **Density profiles reveal interface-induced structure.**

142 Ion behavior in the vicinity of the liquid-vacuum interface was first examined with  
143 density distributions perpendicular to the plane of the interface. Fig. 1 shows the normalized  
144 density along the coordinate perpendicular to the interface for each system considered. The most  
145 obvious difference observed in the simulations is an increase in slab width. This change in width  
146 is directly related to the amount of K, the largest cation considered, in the solution (Fig. 1). Near  
147 the interface there is structure in the densities. The liquid region is flat indicative of  
148 homogeneous liquid structure, the intermediate region between the liquid and vacuum shows two  
149 peaks, and finally there is a drastic decrease in density when moving into the vacuum. The peaks  
150 are most well-defined in the Na-containing systems (red and blue curves in Fig. 1), but these  
151 features are present in each system.

152

### 153 **Slab width and surface tension are highly correlated with system composition.**

154 The width of the slab can be defined as the distance between the Gibbs dividing surface  
155 on each side of the slab (Table 2). The slab width is found to be highly correlated with the size of  
156 the cations. Using ionic radii of 0.68, 0.97, and 1.33 Å for Li, Na, and K cations (Weast, 1968),  
157 an average cation radius can be calculated for each system

$$158 \quad \langle r_{ion} \rangle = \chi^{Li} r_{ion}^{Li} + \chi^{Na} r_{ion}^{Na} + \chi^K r_{ion}^K \quad (1)$$

159 where  $\langle r_{ion} \rangle$  is the average cation radius,  $\chi^X$  is the fraction of the cations that are X, and  $r_{ion}^X$  is  
160 the ionic radius of X. The slab width is found to be highly correlated with the average cation  
161 radius, with a linear coefficient of correlation ( $R^2$ ) of 0.999. The individual cation sizes,  
162 however, are less correlated with slab width. The width is most weakly correlated with the cation  
163 fraction of Li, but significantly stronger correlation is observed with Na and K cation fractions.  
164 The correlation coefficients are 0.780, 0.975, and 0.998 for Li, Na, and K, respectively. These  
165 conclusions are similar to the observation by Habasaki that anion-cation spacing is correlated

166 with the cationic radii of Li and Na in carbonate salts (Habasaki, 1990), which indicates that  
167 molecular-scale spatial correlations can provide a good indication of larger bulk densities.

168 The surface tension can be estimated from the slab width and the diagonal components of  
169 the pressure tensor according to the expression

$$170 \quad \gamma = \frac{L_z}{2} \left( P_{zz} - \frac{1}{2} (P_{xx} + P_{yy}) \right) \quad (2)$$

171 where  $\gamma$  is the surface tension,  $L_z$  is the slab width,  $P_{zz}$  is the component of the pressure tensor  
172 normal to the interface, and  $P_{xx}$  and  $P_{yy}$  are the tangential components of the pressure tensor  
173 (Kirkwood & Buff, 1949). This is similar to the surface tension protocol used by others (Bhatt,  
174 Newman & Radke, 2004; Desmaele et al., 2019). Surface tension values are shown in Table 2  
175 and have not been reported previously for the JT model. Similar to the slab width discussed  
176 previously, the surface tension is found to be highly correlated with K concentration, slightly less  
177 with Na, and significantly less with Li. These values are approximately a quarter of those  
178 reported in the experimental literature (Ward & Janz, 1965; Kojima et al., 2008). The JT model  
179 appears to underestimate cohesive interactions, which is similar to previous studies that have  
180 shown a similar disagreement when the model density is compared to experiment (Ottochian et  
181 al., 2016; Roest et al., 2017; Desmaele et al., 2019). Some works have compensated for this  
182 discrepancy by performing their simulations at elevated pressure (Ottochian et al., 2016; Roest et  
183 al., 2017), but this is not possible here because the liquid is in contact with vacuum and therefore  
184 free to expand. Nevertheless, the literature provides significant evidence that this model provides  
185 a generally faithful description of molten alkali carbonates and as such lends confidence that the  
186 trends reported here are reliable. Additionally, the JT model has received such widespread usage  
187 that characterization of the surface tension provides important perspective on strengths and  
188 weaknesses of the model.

### 189 **Elemental structure at the Gibbs dividing surface.**

190 The normalized density in Fig. 1 includes all species in the system. It is interesting to  
191 decompose the density into the contributions from each species to see if the ions accumulate  
192 differently at the interface. Therefore the density profile of each element was calculated to  
193 resolve these distributions near the interface. For example, the complete density distribution of  
194 each element in the LiNaKCO<sub>3</sub> system is shown in Fig. 2a. Similar to Fig. 1, the densities in Fig.  
195 2 are normalized by dividing by the average density in the middle of the slab. Fig. 2a reveals the

196 anticipated general trend of high density within the slab and no density outside it in the vacuum  
197 and the peaks and valleys indicate interfacial ordering of the individual ions in the elemental  
198 density profiles. This is similar to the entire system density profiles shown in Fig. 1. These  
199 features are difficult to resolve because of the large density difference between the liquid and  
200 vacuum, so Figs. 2b, c, and d show detailed views of the liquid region of the elemental density  
201 profiles for each system. Each element is observed to have maxima and minima induced by  
202 proximity to the interface that are much larger than the subtle, apparently random wiggles in the  
203 middle of the slab. The similarity of the right and left interfaces indicates that the profiles are  
204 converged. Most notably, Na is observed (red lines) to be depleted compared to the other  
205 elements near the Gibbs dividing surface (Figs. 2b and d). In the electrolyte without Na (Fig. 2c),  
206 K is also found to be depleted near the Gibbs dividing surface. The other K-containing solution  
207 (Fig. 2d) does not show similar depletion, but instead K has a significant maximum about 7 Å on  
208 the liquid side of the Gibbs dividing surface. Lithium is generally observed to be the cation with  
209 a maximum closest to the interface, which is generally similar in shape and location to the C  
210 peak of the anion. The C and O peaks are generally similar, with the O showing slightly less  
211 structuring. While some information about ordering of each element relative to the interface is  
212 observed, these features are nevertheless difficult to resolve. Therefore, it would be useful to  
213 further examine the local enrichment or depletion of each species relative to the interface for a  
214 clearer picture of ion distributions.

215 While Fig. 2 shows the structure of each atom at the Gibbs dividing surface in the liquid  
216 region, it is difficult to identify the atomic contributions to the total density profile and more  
217 specifically to see the atomic ordering within the interfacial region. Therefore, Fig. 3 depicts the  
218 difference between Fig. 2b, c, and d and the corresponding total density profiles in Fig. 1. Fig. 3  
219 shows that K has significant density at the surface and is the most prominent, when it is present.  
220 Conversely, as was observed in the analysis of Fig. 2, Na has a major depletion near the interface  
221 compared to its bulk density. The behavior of Li is less dramatic. When K is present, Li has a  
222 peak near the same distance from the interface. When K is not in the solution (Fig. 3a), then Li is  
223 the predominant cation at the Gibbs dividing surface. In all cases, C is depleted at the surface  
224 compared to the cations, but has a maximum just inside the surface. These findings are similar to  
225 those reported by Gutiérrez et al. who also showed ionic structuring near the Gibbs dividing

226 surface (Gutiérrez et al., 2018). Next, these ionic arrangements will be examined further using a  
227 local definition of the interface.

228

### 229 **Instantaneous interface analysis reveals local fluctuations of the liquid surface.**

230 The interfacial analyses so far have been performed with respect to the Gibbs dividing  
231 surface. The Gibbs dividing surface is the plane that on average separates two distinct phases  
232 (Gochenour, Heyert & Lindberg, 2018). The interface, however, need not be viewed as a static  
233 plane, but can also be viewed as a dynamic, three-dimensional region specific to the underlying  
234 molecular configuration. This is similar to the distinction between ‘sea level’ and waves on the  
235 sea, where sea level is determined by averaging over local fluctuations to obtain a useful, but  
236 dramatically simplified, description. Analogously, it is useful to consider an interpretation of the  
237 interface that captures the local molecular-scale undulations. In this work, we utilize the  
238 instantaneous interface scheme developed by Willard and Chandler (Willard & Chandler, 2010).  
239 Briefly, this method involves creating a coarse-grained density field and identifying points in this  
240 coarse grained density field at a density halfway between that of the two phases. These points  
241 can then be connected to identify the interface that separates the two phases. The long time  
242 average of the instantaneous interface is analogous to the Gibbs dividing surface. An example of  
243 such an instantaneous interface is shown for the  $\text{LiKCO}_3$  system in Fig. 4. In this work, we use  
244 the instantaneous interface to characterize fluctuations of the surface and elemental distributions  
245 in the vicinity of the instantaneous interface.

246

### 247 **Elemental structure at the instantaneous interface shows cations preferentially populate** 248 **the surface.**

249 The instantaneous interface corresponds to the boundary between the molten salt liquid  
250 and vacuum for a particular molecular configuration. Therefore, analysis of the instantaneous  
251 interface and the underlying atomic distribution provides details about the behavior of the system  
252 in light of a specific arrangement of the atoms, rather than the time-averaged, global behavior  
253 described by the Gibbs dividing surface. Fig. 5 shows a histogram of the instantaneous interface  
254 with respect to the Gibbs dividing surface. The instantaneous interface is found to not be  
255 symmetric or symmetrically distributed around the Gibbs dividing surface. Instead the  
256 asymmetric distribution has a maximum beyond the Gibbs dividing surface with a long tail

257 extending into the liquid regime. Depending on the system, the instantaneous interface is found  
258 to extend between 5 to 10 Å into the liquid region. This is in agreement with the structure  
259 observed in Fig 3, which shows structure in the atomic density distributions to approximately 10  
260 Å into the liquid. There are differences between the solutions considered, with the  $\text{LiNaCO}_3$   
261 solution having the least pronounced skewness extending into the liquid and  $\text{LiKCO}_3$  the most,  
262 which provides an estimate of the size of the interfacial region. It would be expected that larger  
263 solution surface tensions would correspond to a greater energy associated with deformation from  
264 a minimum surface area, but it appears that the differences in surface tension are not large  
265 enough to have a clear effect on the distribution of instantaneous interface sites.

266 Fig. 6 shows a histogram of the shortest distance between each element and the  
267 instantaneous interface. The curves are normalized so they all have maximum values of 1 to  
268 simplify comparisons between species, despite different concentrations. The density profiles  
269 relative to the instantaneous interface in Fig. 6 provide a complementary perspective on ion  
270 structure near the interface to those observed with respect to the Gibbs dividing surface in Figs 2  
271 and 3. In Fig. 6, the cations are always more likely to be closer to the instantaneous interface  
272 than the anions. The ordering is distinct, with K being closest, then Na, Li, O, and finally C. It is  
273 interesting to note that the cation trend inversely follows the ionic radii. This indicates that the  
274 cations preferentially populate the surface of the instantaneous interface. Interestingly, these  
275 distributions are apparently independent of the electrolyte composition, and therefore possibly  
276 indicative of broader trends in ion behavior in these molten alkali carbonate electrolytes. The  
277 uniformity of the elemental distributions in each panel of Fig. 6 is distinct from the behavior  
278 observed with respect to the Gibbs dividing surface shown in Figs. 2 and 3. This indicates that  
279 the dynamics of the interface can be affected by the composition, but the actual arrangement of  
280 the atoms is less sensitive.

281

### 282 **Anions diffuse slower than the cations.**

283 Finally, the transport of the ions is evaluated using the self-diffusion constants. Table 3  
284 shows the diffusion constant of each species in each system. The diffusion constants are in  
285 general agreement with previous, similar studies (Habasaki, 1990; Koishi et al., 2000; Costa,  
286 2008; Vuilleumier et al., 2014; Ottochian et al., 2016; Corradini, Coudert & Vuilleumier, 2016;  
287 Roest et al., 2017), however exact comparison with bulk diffusion constants is difficult since the

288 systems described here are heterogeneous. Nevertheless, this work shows that carbonate diffuses  
289 slower than all of the cations. The cation self-diffusion is found to be proportional to cation size,  
290 with the larger ions diffusing faster. This is attributed to each cation having the same charge, so  
291 larger radii ions experience correspondingly weaker electrostatic interactions.

292

## 293 CONCLUSIONS

294 Molecular dynamics simulations have revealed thermodynamic and dynamic properties  
295 of molten alkali carbonates near a liquid-vacuum interface. This work has shown that in three  
296 alkali carbonate salts, the alkali cations preferentially accumulate at the interface more than the  
297 anion. Additionally, the anions are found to diffuse much more slowly than the cations.  
298 Nevertheless, subtle differences are seen between the three solutions considered, which may be  
299 helpful in the selection of electrolyte compositions that yield the best performance in an  
300 electrochemical device. Intriguingly, the  $\text{LiKCO}_3$  solution is found to yield the fastest carbonate  
301 diffusion while also permitting the closest approach of the anion to the interface. These  
302 differences could have significant effects on the performance of devices employing such  
303 electrolytes and therefore warrant study to understand and confirm these results.

304

## 305 CONFLICTS OF INTEREST

306 There are no conflicts to declare.

307

## 308 ACKNOWLEDGEMENTS

309 This work employed Northern Arizona University's Monsoon computing cluster, which is  
310 funded by Arizona's Technology and Research Initiative Fund.

311

## 312 REFERENCES

- 313 Allara DL. 2005. A perspective on surfaces and interfaces. *Nature* 437:638–639.
- 314 Bastos-González D, Pérez-Fuentes L, Drummond C, Faraudo J. 2016. Ions at interfaces: the  
315 central role of hydration and hydrophobicity. *Current opinion in colloid & interface science*  
316 23:19–28.

- 317 Bhatt D, Newman J, Radke CJ. 2004. Molecular Dynamics Simulations of Surface Tensions of  
318 Aqueous Electrolytic Solutions. *The journal of physical chemistry. B* 108:9077–9084.
- 319 Corradini D, Coudert F-X, Vuilleumier R. 2016. Insight into the Li<sub>2</sub>CO<sub>3</sub>-K<sub>2</sub>CO<sub>3</sub> eutectic  
320 mixture from classical molecular dynamics: Thermodynamics, structure, and dynamics. *The*  
321 *Journal of chemical physics* 144:104507.
- 322 Costa MF. 2008. Molecular dynamics of molten Li<sub>2</sub>CO<sub>3</sub>-K<sub>2</sub>CO<sub>3</sub>. *Journal of molecular liquids*  
323 138:61–68.
- 324 Desmaele E, Sator N, Vuilleumier R, Guillot B. 2019. Atomistic simulations of molten  
325 carbonates: Thermodynamic and transport properties of the Li<sub>2</sub>CO<sub>3</sub>-Na<sub>2</sub>CO<sub>3</sub>-K<sub>2</sub>CO<sub>3</sub>  
326 system. *The Journal of chemical physics* 150:094504.
- 327 Dicks AL. 2004. Molten carbonate fuel cells. *Current Opinion in Solid State and Materials*  
328 *Science* 8:379–383.
- 329 Ding J, Du L, Pan G, Lu J, Wei X, Li J, Wang W, Yan J. 2018. Molecular dynamics simulations  
330 of the local structures and thermodynamic properties on molten alkali carbonate K<sub>2</sub>CO<sub>3</sub>.  
331 *Applied energy* 220:536–544.
- 332 Du L, Ding J, Wang W, Pan G, Lu J, Wei X. 2017. Molecular dynamics simulations on the  
333 binary eutectic system Na<sub>2</sub>CO<sub>3</sub>-K<sub>2</sub>CO<sub>3</sub>. *Energy Procedia* 142:3553–3559.
- 334 Du L, Xie W, Ding J, Lu J, Wei X, Wang W. 2019. Molecular dynamics simulations of the  
335 thermodynamic properties and local structures on molten alkali carbonate Na<sub>2</sub>CO<sub>3</sub>.  
336 *International journal of heat and mass transfer* 131:41–51.
- 337 Gaune-Escard M, Haarberg GM. 2014. *Molten Salts Chemistry and Technology*. Chichester, UK:  
338 John Wiley & Sons, Ltd.
- 339 Gochenour K, Heyert AJ, Lindberg GE. 2018. Molecular Simulations of Volatile Organic

- 340 Interfaces. In: Faust JA, House JE eds. *Physical Chemistry of Gas-Liquid Interfaces*.  
341 Elsevier, 41–58.
- 342 Gutiérrez A, Garroni S, Souentie S, Cuesta-López S, Yakoumis I, Aparicio S. 2018. Theoretical  
343 Study on Molten Alkali Carbonate Interfaces. *Langmuir: the ACS journal of surfaces and*  
344 *colloids* 34:13065–13076.
- 345 Gutiérrez A, Garroni S, Souentie S, Cuesta-López S, Yakoumis I, Aparicio S. 2019. Insights into  
346 Carbon Nanotubes and Fullerenes in Molten Alkali Carbonates. *Journal of Physical*  
347 *Chemistry C* 123:9909–9918.
- 348 Habasaki J. 1990. Molecular dynamics simulation of molten  $\text{Li}_2\text{CO}_3$  and  $\text{Na}_2\text{CO}_3$ . *Molecular*  
349 *physics* 69:115–128.
- 350 Humphrey W, Dalke A, Schulten K. 1996. VMD: visual molecular dynamics. *Journal of*  
351 *molecular graphics* 14:33–8, 27–8.
- 352 Janssen GJM, Tissen JTWM. 1990. Pair Potentials from ab initio Calculations for use in MD  
353 Simulations of Molten Alkali Carbonates. *Molecular simulation* 5:83–98.
- 354 Janz GJ. 1967. Molten carbonate electrolytes as acid-base solvent systems. *Journal of chemical*  
355 *education* 44:581.
- 356 Kirkwood JG, Buff FP. 1949. The Statistical Mechanical Theory of Surface Tension. *The*  
357 *Journal of chemical physics* 17:338–343.
- 358 Kirubakaran A, Jain S, Nema RK. 2009. A review on fuel cell technologies and power electronic  
359 interface. *Renewable and Sustainable Energy Reviews* 13:2430–2440.
- 360 Koishi T, Kawase S, Tamaki S, Ebisuzaki T. 2000. Computer Simulation of Molten  $\text{Li}_2\text{CO}_3$ -  
361  $\text{K}_2\text{CO}_3$  Mixtures. *Journal of the Physical Society of Japan* 69:3291–3296.
- 362 Kojima T, Miyazaki Y, Nomura K, Tanimoto K. 2008. Density, Surface Tension, and Electrical

- 363 Conductivity of Ternary Molten Carbonate System  $\text{Li}_2\text{CO}_3 - \text{Na}_2\text{CO}_3 - \text{K}_2\text{CO}_3$  and  
364 Methods for Their Estimation. *Journal of the Electrochemical Society* 155:F150–F156.
- 365 Kumar R, Knight C, Voth GA. 2013. Exploring the behaviour of the hydrated excess proton at  
366 hydrophobic interfaces. *Faraday discussions* 167:263–278.
- 367 Maru HC. 1984. Alkali Metal Carbonates. In: *Molten Salt Techniques*. Springer US, 15–43.
- 368 Ottochian A, Ricca C, Labat F, Adamo C. 2016. Molecular dynamics simulations of a  
369 lithium/sodium carbonate mixture. *Journal of molecular modeling* 22:61.
- 370 Plimpton S. 1995. Fast Parallel Algorithms for Short-Range Molecular Dynamics. *Journal of*  
371 *computational physics* 117:1–19.
- 372 Roe DR, Cheatham TE. 2013. PTRAJ and CPPTRAJ: Software for Processing and Analysis of  
373 Molecular Dynamics Trajectory Data. *Journal of chemical theory and computation* 9:3084–  
374 3095.
- 375 Roest DL, Ballone P, Bedeaux D, Kjelstrup S. 2017. Molecular Dynamics Simulations of  
376 Metal/Molten Alkali Carbonate Interfaces. *Journal of Physical Chemistry C* 121:17827–  
377 17847.
- 378 Soniat M, Kumar R, Rick SW. 2015. Hydrated proton and hydroxide charge transfer at the  
379 liquid/vapor interface of water. *The Journal of chemical physics* 143:044702.
- 380 Tissen JTWM, Janssen GJM. 1990. Molecular-dynamics simulation of molten alkali carbonates.  
381 *Molecular physics* 71:413–426.
- 382 Tissen JTWM, Janssen GJM, Eerden P van der. 1994. Molecular dynamics simulation of binary  
383 mixtures of molten alkali carbonates. *Molecular physics* 82:101–111.
- 384 Tse Y-LS, Chen C, Lindberg GE, Kumar R, Voth GA. 2015. Propensity of Hydrated Excess  
385 Protons and Hydroxide Anions for the Air-Water Interface. *Journal of the American*

- 386 *Chemical Society* 137:12610–12616.
- 387 Vuilleumier R, Seitsonen A, Sator N, Guillot B. 2014. Structure, equation of state and transport  
388 properties of molten calcium carbonate (CaCO<sub>3</sub>) by atomistic simulations. *Geochimica et*  
389 *cosmochimica acta* 141:547–566.
- 390 Wade JL, Lee C, West AC, Lackner KS. 2011. Composite electrolyte membranes for high  
391 temperature CO<sub>2</sub> separation. 369:20–29.
- 392 Ward AT, Janz GJ. 1965. Molten carbonate electrolytes: Electrical conductance, density and  
393 surface tension of binary and ternary mixtures. *Electrochimica acta* 10:849–857.
- 394 Weast RC (ed.). 1968. *CRC Handbook of Chemistry & Physics 49TH Edition*. The Chemical  
395 Rubber Co.
- 396 Wilding MC, Wilson M, Alderman OLG, Benmore C, Weber JKR, Parise JB, Tamalonis A,  
397 Skinner L. 2016. Low-Dimensional Network Formation in Molten Sodium Carbonate.  
398 *Scientific reports* 6:24415.
- 399 Willard AP, Chandler D. 2010. Instantaneous liquid interfaces. *The journal of physical*  
400 *chemistry. B* 114:1954–1958.

**Table 1** (on next page)

Salt cation fractions used in this work.

1 Table 1: Cation fractions for the eutectic salts used in this work.

System	Li	Na	K
LiNaKCO <sub>3</sub>	0.435	0.315	0.25
LiNaCO <sub>3</sub>	0.53	0.47	0
LiKCO <sub>3</sub>	0.427	0	0.573

2

**Table 2** (on next page)

Width and surface tension for each of the systems studied.

1 Table 2: Width and surface tension for each of the systems studied.

System	Width (Å)	Surface tension (mN/m)
LiNaCO <sub>3</sub>	30.7	39.37±0.09
LiKCO <sub>3</sub>	39.0	50.0±0.1
LiNaKCO <sub>3</sub>	34.6	44.4±0.1

2

**Table 3** (on next page)

Self-diffusion constants of each ion in each of the systems studied.

1 Table 3: Self-diffusion constants of each ion in each of the systems studied.

System	Li ( $\text{\AA}^2/\text{ps}$ )	Na ( $\text{\AA}^2/\text{ps}$ )	K ( $\text{\AA}^2/\text{ps}$ )	C ( $\text{\AA}^2/\text{ps}$ )
LiNaCO <sub>3</sub>	4.0±0.3	4.4±0.4	--	1.5±0.1
LiKCO <sub>3</sub>	3.3±0.3	--	4.5±0.3	1.8±0.2
LiNaKCO <sub>3</sub>	3.2±0.3	3.8±0.3	4.2±0.4	1.5±0.1

2

## Figure 1

Normalized total density profile in the dimension perpendicular to the interface.

The densities are normalized by dividing by the average liquid density. For each system, the right Gibbs dividing surface is positioned at 0 Å and the left interface provides a sense of the slab width because the xy area of the slab remains constant. Expansion of the slab is highly correlated with increasing concentration of the larger radius K ion. Each system shows structure near each interface that corresponds to structure within the liquid.

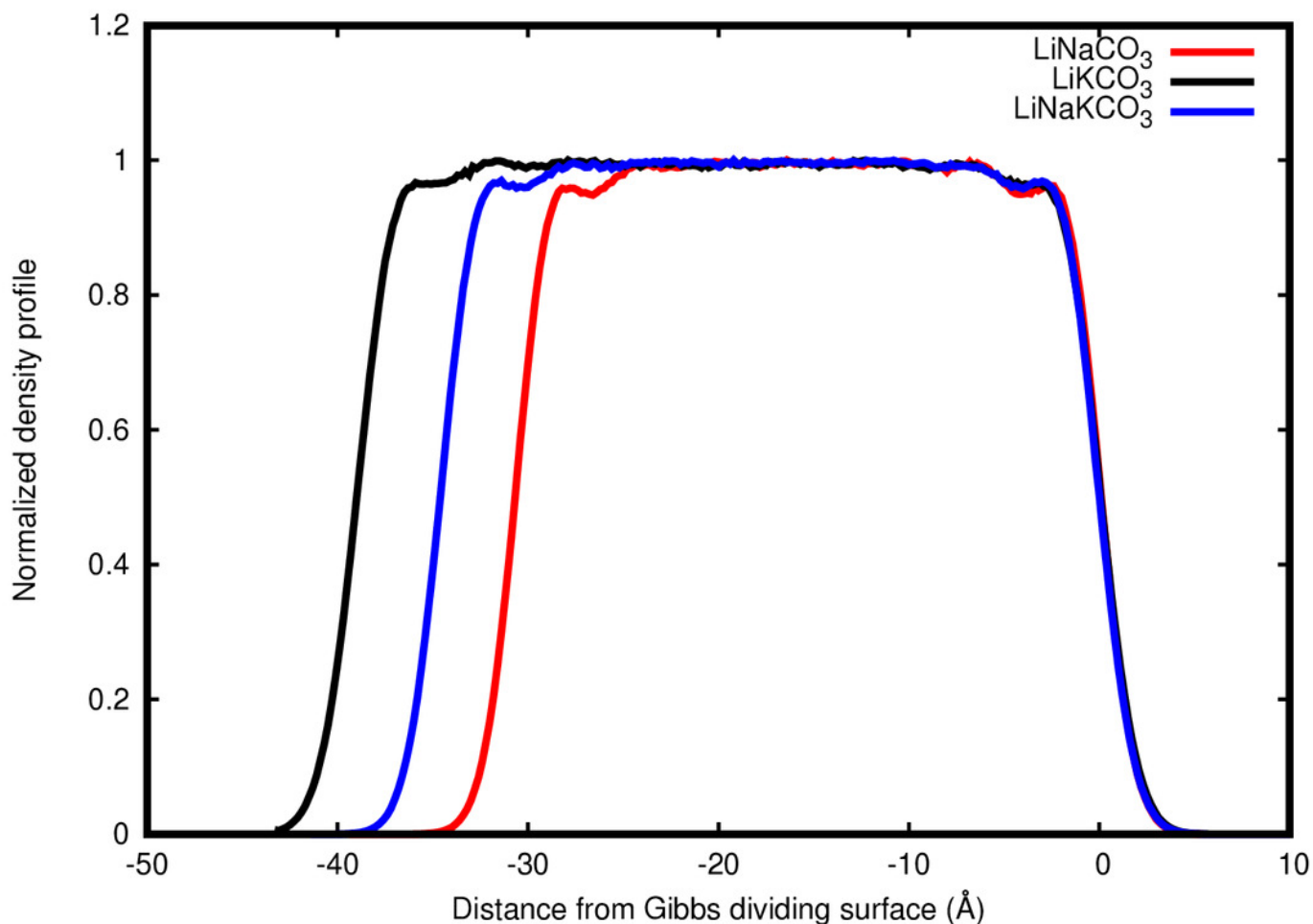


## Figure 2

Normalized densities with respect to the right Gibbs dividing surface.

Shown for Li (green), Na (red), K (black), C (orange), and O (blue) in the a) entire  $\text{LiNaKCO}_3$  system and detailed views of the liquid region for b)  $\text{LiNaCO}_3$ , c)  $\text{LiKCO}_3$ , and d)  $\text{LiNaKCO}_3$ . For each system, the right Gibbs dividing surface is positioned at  $0 \text{ \AA}$ . The peaks and valleys are indicative of the atomic structuring near the surface.

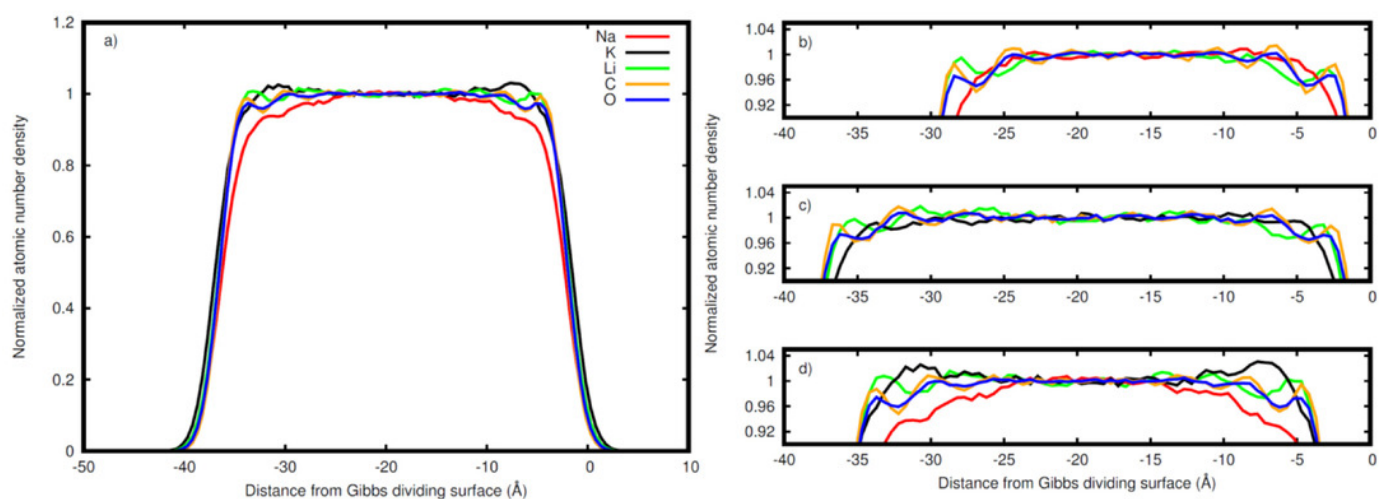


## Figure 3

Atomic density differences from the total density profile in the dimension perpendicular to the Gibbs dividing surface.

Shown for Li (green), Na (red), K (black), C, (orange), and O (blue) for the a)  $\text{LiNaCO}_3$ , b)  $\text{LiKCO}_3$ , and c)  $\text{LiNaKCO}_3$  systems. These are the profiles in Fig. 2 with the whole system profiles in Fig. 1 subtracted. These plots emphasize the contributions of each element to the total density profile. For each system, the right Gibbs dividing surface is positioned at 0 Å.

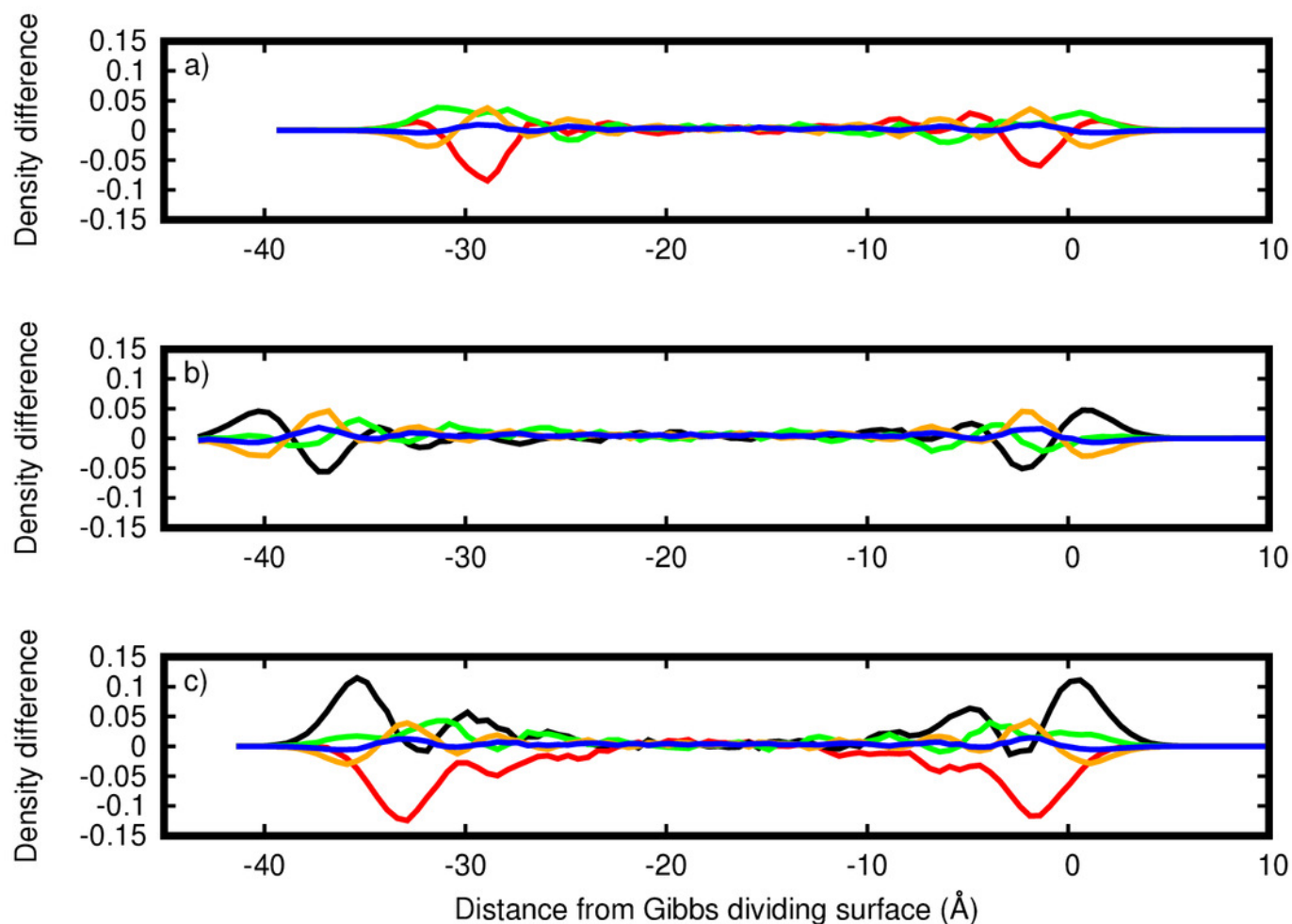


## Figure 4

A representative snapshot of the  $\text{LiKCO}_3$  system with the corresponding instantaneous interface.

The atoms comprising the salt are depicted in green, purple, blue, and pink and the instantaneous interface is shown in gold.

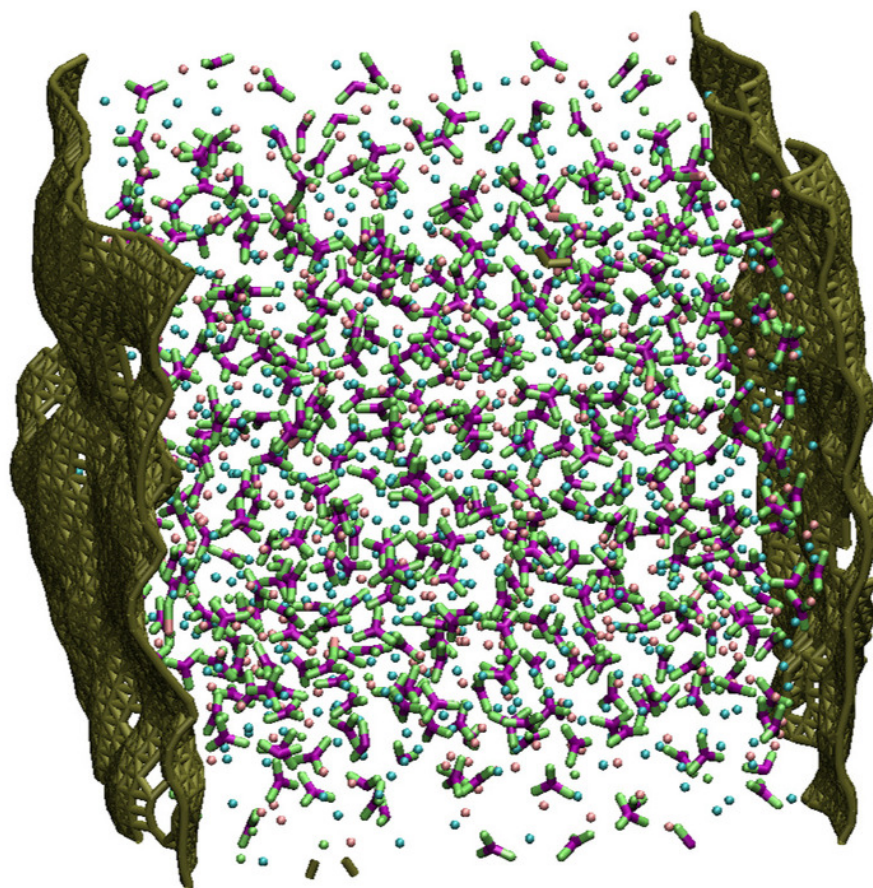


## Figure 5

Distribution of instantaneous interface sites relative to the Gibbs dividing surface.

Shown are  $\text{LiNaCO}_3$  (red),  $\text{LiKCO}_3$  (black), and  $\text{LiNaKCO}_3$  (blue).

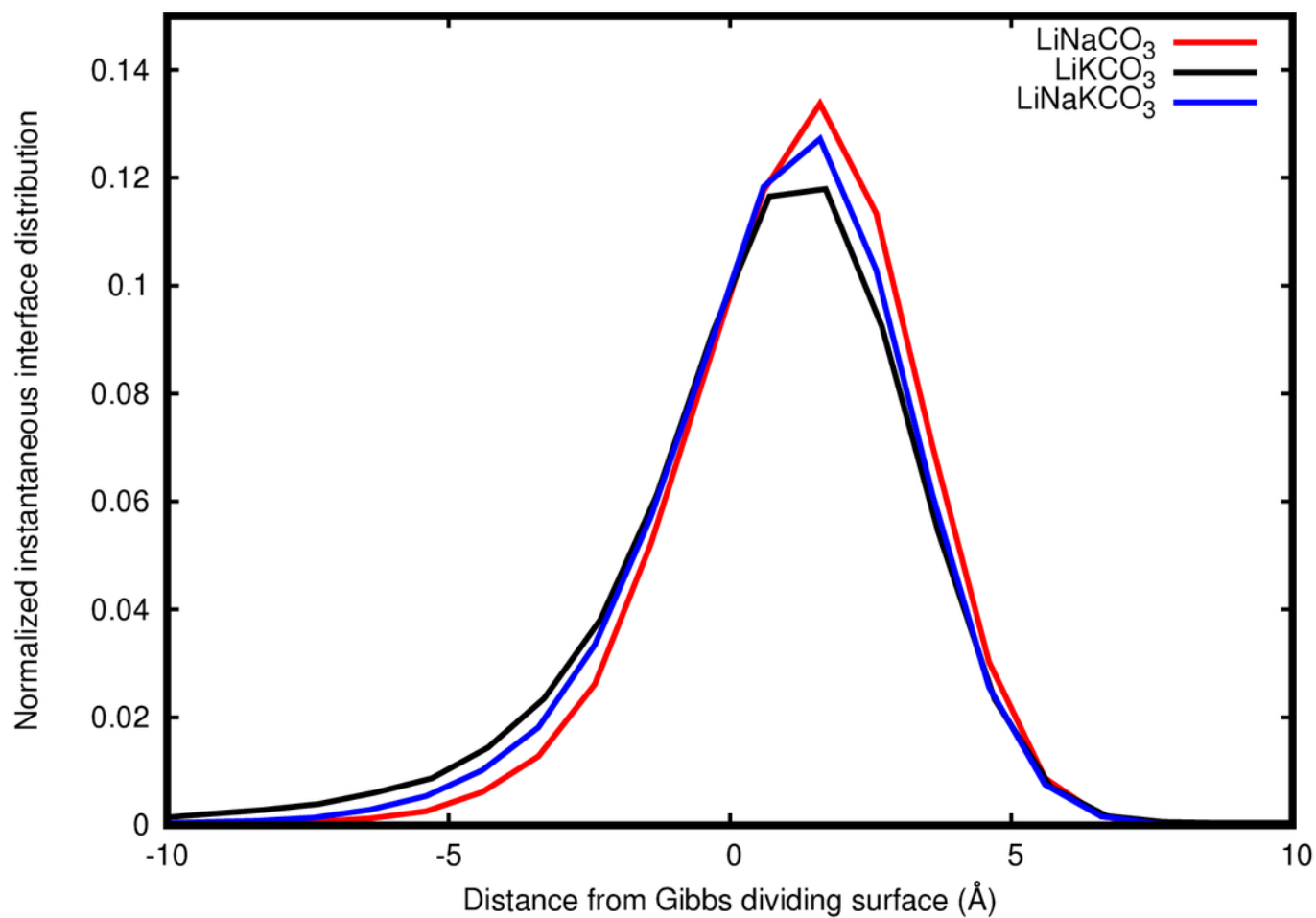


## Figure 6

Normalized histogram of the distance of each element from the closest point on the instantaneous interface.

Shown Li (green), Na (red), K (black), C (orange) and O (blue) for the a)  $\text{LiNaCO}_3$ , b)  $\text{LiKCO}_3$ , and c)  $\text{LiNaKCO}_3$  systems.

